SOME EFFECTS OF NUCLEAR FORCES ON NEUTRON STAR MODELS

by

Sachiko Tsuruta

Smithsonian Astrophysical Observatory
Cambridge, Massachusetts

Physics Department, Columbia University
New York, New York

and

Institute for Space Studies
Goddard Space Flight Center, NASA
New York, New York

and

A.G.W. Cameron

Institute for Space Studie
Goddard Space Flight Center, NASA
New York, New York

ABSTRACT

Two composite equations of state have been used in
the investigation of the structure of neutron (or hy-
peron or baryon) stars. These have been based upon
two forms of the neutron-neutron potential suggested
by Levinger and Simmons. In one form repulsive forces
come in quickly at greater than nuclear densities; in the
other form the repulsive forces come in slowly. In the
former case the maximum stable mass of a neutron star is
about two solar masses; whereas in the latter case it
is only about one solar mass. This probably represents
a measure of the basic uncertainty in the properties
of neutron star models due to our lack of knowledge of
nuclear forces. The maximum central density of a stable
configuration is similarly uncertain; this density
probably lies in the range 10^{15} to 10^{16} grams/cm^3.
Details of many of the neutron star models calculated
are summarized and discussed.

INTRODUCTION

The problem of the properties of highly condensed matter has a long history. The first important contributions came as early as in the period of 1930-40, from Chandrasekhar (1935, 1939), Landau (1932), Oppenheimer and Serber (1938), Oppenheimer and Volkoff (1939), and others. For a degenerate body under gravitational attraction there may exist two possible equilibrium states, the less condensed state composed of electrons and nuclei, and the more compressed state of neutronic or baryonic configuration. The "electron-nuclear" state corresponds to the observed white dwarf stars. It was suggested (Zwicky 1938, 1939, and 1958) that the more condensed state of nuclear density might be physically realized in a form of a neutron star formed as the result of a supernova explosion, at the last stage of evolution of a sufficiently massive star. This view was somewhat neglected for a long time. However, there has recently arisen a possibility that a neutron star formed as a remnant of a supernova explosion may directly or indirectly be responsible for some of the celestial x-ray sources now known to exist (Chiu 1964, Chiu and Salpeter 1964, Morton 1964, Tsuruta 1964, Cameron 1965, and others), and the importance of the study of highly condensed matter has been greatly increased. Even aside from the problem of observing

these stars, the study of degenerate stars is important in itself
as a fundamental problem in physics. J.A. Wheeler and his
collaborators have been pursuing the problem of degenerate stars
since 1958 in connection with gravitation theory and gravitational
collapse. The best collection of their work is found in Harrison,
Thorne, Wakano and Wheeler (1965). Some other recent contributions to
this problem are those of Cameron (1959), Amburtsumyan and Saakyan (1960,
1962, a,b), Sahakian and Vartaman (1963), and Misner and Zapolsky (1964).

In considerations of neutron stars the greatest uncertainty
is caused by lack of knowledge of high energy physics, and, for
this reason, the interaction forces between neutrons were usually
neglected in most of the previous work. However, the typical
density in neutron stars is as high as $\sim 10^{15}$ gm/cm^3 or more,
for which the nuclear forces between the constituent particles
are far too important to be neglected. It should be emphasized
that an exact knowledge of the nuclear forces near and just above
nuclear densities (around $10^{14} \leqslant \rho \leqslant 10^{16}$ gm/cm^3) is required
to determine the quantitative properties of the models not only
in this range but also for far denser configurations. It is
likely that denser matter, $\rho > 10^{16}$ gm/cm^3, should follow a
simple asymptotic equation of state of the polytropic form
$P = cn^\gamma = (\gamma-1)\epsilon$, with the value of γ properly chosen (where
P is the pressure, c is a constant, γ is the adiabatic exponent

and ϵ is the energy density), but the important question is:
to what nuclear equation of state should this be joined in the
lower density region near the surface? Some efforts have been
made in recent years to take into account these nuclear forces
by Cameron (1959), Amburtsumyan and Saskaan (1962a) and others.
In this paper we explore this problem in more detail.

For this purpose, we have chosen two possible forms of the
nuclear interaction between neutrons as suggested by Levinger and
Simmons (1961). The possible application of these nuclear potentials
to the problem of neutron stars was proposed by Salpeter (1963).
These potentials are consistant with our knowledge of nuclear
forces in the vicinity of normal nuclear densities, if we
assume charge independence of these forces. However, the uncer-
tainty is increased as the density goes higher. Hence, the
difference in the models constructed by the use of these two
different nuclear potentials may give an indication of the
uncertainty due to the lack of knowledge in this field.
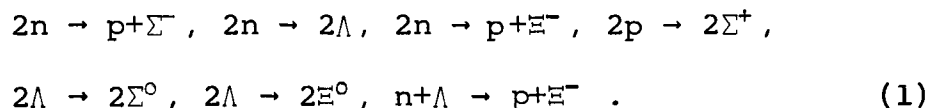
In a physically realistic equation of state the pressure
is not allowed to become indefinitely large. Therefore, either
one of the possible pressure saturation conditions $P \leq \epsilon/3$
(Landau and Lifshitz 1959) or $P \leq \epsilon$ (Zel'dovich 1962) were
applied in our models. In our composite equation of state the
equilibrium composition of degenerate matter was used. For

densities lower than about 3×10^{11} gm/cm^3 matter consists of degenerate electrons and various heavy nuclei. The most abundant nucleus changes from iron to more neutron-rich nuclei with increasing density (Tsuruta and Cameron 1965). For densities higher than this, heavy ions gradually disolve into neutrons. The system then consists of neutrons, protons and electrons in equilibrium. Near and above 10^{15} gm/cm^3, mesons and other baryons appear. The threshold density at which these new particles appear is quite uncertain due to the lack of knowledge of the interaction forces between the strongly interacting particles. However, as will be shown later, the effect of the possible change of composition due to the shifting of the threshold energy for the appearance of these particles is very small. At the present stage, we are very ignorant concerning the quantitative nature of the strong interaction forces between hyperons, but we know that these forces are of the same nature as the nuclear forces which are responsible for the binding of nucleons together in a nucleus. Hence it was assumed that the same Levinger-Simmons type nuclear potentials were experienced by all the nucleons and hyperons which are present in the assembly.

This paper is confined to cold models of degenerate stars. The cooling of such stars will be treated in a separate paper.

HYPERONIC MIXTURES

When densities exceed about 3×10^{11} gm/cm^3, all heavy ions become unstable against disintegration to neutrons by means of electron capture, and matter consists mainly of neutrons. These neutrons are, however, unstable against decay to protons and electrons by 0.783 Mev, the neutron-hydrogen mass difference, and the neutron gas is always contaminated with protons and electrons. When the Fermi energy of the electrons reaches the rest mass of the muon, 106 Mev, neutrons can be transformed into protons and negative muons. With further increase of energy, various kinds of hyperons are created. Some of the many possible hyperon production reactions are:

$$2n \rightarrow p+\Sigma^-, \quad 2n \rightarrow 2\Lambda, \quad 2n \rightarrow p+\Xi^-, \quad 2p \rightarrow 2\Sigma^+,$$
$$2\Lambda \rightarrow 2\Sigma^\circ, \quad 2\Lambda \rightarrow 2\Xi^\circ, \quad n+\Lambda \rightarrow p+\Xi^- . \tag{1}$$

We note that in these reactions strangeness is not conserved. The time scale of processes like (1) is on the order of 10^{-9} sec, which is long compared with nuclear time scales but extremely short from the astronomical point of view. Even though faster reactions exist, the above examples are fast enough to maintain equilibrium. Consequently we can safely assume that thermodynamic equilibrium is maintained throughout.

The densities at which these meson and hyperon transformations take place are above nuclear densities, and all the constituent baryons and leptons become highly degenerate soon after creation at the threshold energy. Even when the temperature is as high as 5×10^9 $^{\circ}$K (a typical maximum temperature of interest in the problem of neutron stars) their degeneracy is so high that the cold matter approximation is fully justified. (For instance, at $T = 5 \times 10^9$ $^{\circ}$K and $\rho = 10^{15}$ gm/cm^3, the ratio of neutron Fermi energy to kT is about 400). Therefore, we can assume that all the constituent particles are in their lowest energy states.

Some years ago we had a rather tidy list of about 30 so-called "elementary" particles. Today 60 to 70 more have been added. The first problem we face is to determine which of this profusion of particles survive as the authentic components of our baryon gas in our range of interest. First of all, positrons, photons, neutrinos, positive muons and pions, and K mesons are all absent at zero temperatures because nothing prevents their decay and annihilation. On the other hand, stability is established among hyperons, nucleons, negative muons and electrons, because the decay products of these particles find no unoccupied place in phase space due to the complete degeneracy of baryons and electrons and the Pauli exclusion principle. The stability of

negative pions is established through the high degeneracy of negative muons at very high densities. The presence of the newly discovered particles is restricted due to the fact that most of these particles are heavier states of familiar mesons, nucleons, and hyperons, and that the upper limit of density of interest to us is about 10^{16} gm/cm^3. This is because the equation of state for densities higher than this value becomes independent of the kind and the concentration of particles present as explained in the next section. Consequently, the following thirteen particles were selected as sufficient for our investigation, following Ambartsumyan and Saakyan (1960):

$$e^-, \ \mu^-, \ p, \ p*, \ n, \ n*, \ \Lambda, \ \Sigma^0, \ \Sigma^+, \ \Sigma^-, \ \Xi^0, \ \Xi^-, \ \pi^- \qquad (2)$$

n* and p* are isobars of neutrons and protons in the first excited states, now called delta particles.

The concentration and the threshold energy of the appearance of each of these particles are determined by minimizing the total energy subject to the constraints of conservation of charge and baryon number. The results may be expressed as:

$$E_b^+ + E_e = E_b^- - E_e = E_b^0 \qquad (3a)$$

$$E_\ell^- = E_e = E_\pi^- \qquad (3b)$$

$$\Sigma \ n_b = n \qquad (3c)$$

$$\sum_b \ n_b^+ - \sum_b \ n_b^- - \sum_\ell \ n_\ell^- - n_\pi^- - n_e = 0 \qquad (3d)$$

where E and n represent the total energy and total number density. The superscripts +, -, and 0 refer to individual positive, negative, and neutral particles, and the subscripts b, ℓ, π and e refer to baryons, leptons excluding electrons, pions, and electrons. The first two equations correspond to thermodynamic equilibrium and the last two equations represent the conservation of baryon number and the conservation of electric charge, respectively. In a macroscopic medium consisting of sub-atomic particles, only the average potential energy of the particle is worth mentioning, as it represents the interaction of one particle with all the others. In such a case, the total energy E_k of completely degenerate fermions k can be expressed as

$$E_k = \left[M_k^2 c^4 + \left(p_k^F \right)^2 c^2 \right]^{1/2} + V_k \qquad (4)$$

where

$$p_k^F = \left(\frac{6\pi^2}{a_k} \right)^{1/3} \hbar \, n_k^{1/3}$$

is the Fermi momentum, M_k is the mass, and V_k is the average interaction potential of the particles k. (a_k is as defined in (5)). The first two terms represent the chemical potential. For completely degenerate bosons the chemical potential is just the rest mass of the particle. The present state of the theory of elementary particles is so far in no position to give any definite information on the inter-

action potentials of strongly interacting particles for densities
substantially exceeding nuclear density. Hence, at present we
do not know how to improve upon the simple assumption that all
baryons interact identically (that is, V_k for all baryons are
equal). We neglect V_k in calculating the composition of the
medium, but not its pressure. Interaction potentials of leptons
can always be neglected in the problem of neutron stars (Salpeter,
1961). The concentration n_k of the particles k in a hyperonic
mixture may then be found from

$$n_k = \frac{1}{2} a_k n_i \left[1 - (A_k^i/n_i)^{2/3} \right]^{3/2} \tag{5}$$

where

$$A_k^i = \frac{1}{3\pi^2 \lambda_k^3} \left[1 - (M_i/M_k)^2 \right]^{3/2}$$

$\lambda_k = \hbar/(M_k c)$, M_k is the mass of a particle k,

$a_k = 2I_k + 1$, I_k = the spin of the particle k,

$[I_k = 3/2$ for $n*$ and $P*$, $I_k = \frac{1}{2}$ for others in (2)$]$

$i = e^-$ when $k = \mu^-$

$i = n$ when $k = \Lambda$, Σ^0, Ξ^0 or $n*$,

$i = P$ when $k = \Sigma^+$ or $P*$, and

$i = \Sigma^-$ when $k = \Xi^-$.

When $n_i \leq A_k^i$ no particles k exist and therefore A_k^i is the threshold

number density of the particles i for the creation of particles k.

The numbers of muons are expressed in terms of electron numbers,

the numbers of the positively charged baryons are expressed in

terms of proton numbers, those of negatively charged baryons Ξ^-

are expressed in terms of Σ^-, and the numbers of neutral baryons

are expressed in terms of neutrons. Hence equations (5) give

the concentration of all particles k as a function of neutron

number density n_n, if the number densities of electrons, protons

and Σ^-, n_e, n_p, and n_{Σ^-}, are known as a function of n_n. These

are determined from

$$E_p + E_e = E_n$$

$$E_{\Sigma^-} - E_e = E_n \qquad (6)$$

and the last two equations in (3). This problem was solved by

an iterative procedure. Once the concentrations of the constituent

particles are known, the total density of matter is found from

$$\rho = \sum_k n_k M_k \qquad (7)$$

where the summation is taken over all particles k which are present.

When the threshold energies of electrons and negative muons

exceed the rest mass of negative pions it is more economical

energetically if e^- and μ^- are converted to π^-. In this case,

the number densities of e^- and μ^- stay constant with further increase in total density, at the values

$$n_e = 1.2 \times 10^{37} \text{ cm}^{-3} = (3\pi^2 \lambdabar_\pi^3)^{-1}$$

$$n_\mu = 3.36 \times 10^{36} \text{ cm}^{-3} = \frac{c^3}{3\pi^2} (m_\pi^2 - m_\mu^2)^{3/2}/\hbar^3 . \tag{8}$$

This is because all the excess electrons and μ^- above the threshold value are converted to π^- in a higher density region.

When the electron threshold energy is lower than the muon rest energy, but when the sum of the proton and electron theshold energies is larger than the neutron rest energy, the abundance equations take the simpler form:

$$n_p = n_e = n_o \chi^{-3} \{ [1 + \alpha\chi/\pi + \chi^2 (n_n/n_o)^{2/3}]^{1/2} - 1 \}^3$$

with

$$\alpha = (M_n - M_p)/m_e = 2.54; \quad \chi = 2\pi m_e/M_p,$$
$$n_o = 8(m_e c/\hbar)^3 = 8/\lambdabar_e^3 \tag{9}$$

and

$$\rho = M_p n_p + M_n n_n$$

For densities lower than $\sim 3 \times 10^{11}$ gm/cm^3, the equilibrium nuclear abundances of various heavy nuclei as calculated by Tsuruta and Cameron (1965) apply.

The results are summarized in Figure 1. The number densities of various baryons k are plotted as functions of the total density ρ. For $\rho \leqslant 10^{15}$ gm/cm^3 the total baryon number density and nuetron number density practically coincide. For $\rho \gtrsim 3 \times 10^{15}$ gm/cm^3 the rapid rise in the densities of other baryons depresses the neutron density considerably below the total baryon density. For densities higher than about 5×10^{16} gm/cm^3 the concentrations of all kinds of baryons are about $10^{39} - 10^{40}$ cm^{-3} and they are all of the same order of magnitude. The electrons and μ^- densities exhibit a sudden drop a little above $\rho = 10^{15}$ gm/cm^3, where the Σ^- hyperons appear. n_e and n_μ become constant around $\rho = 10^{17}$ gm/cm^3, due to the creation of π^- mesons.

It may be worthwhile to note that the order in which the particles appear is not in the order of increasing masses. For instance, Σ^- is heavier than Λ, but Σ^- begins to appear at lower densities than Λ. The reason is that the Σ^- hyperons have to neutralize the positive charge of the protons whose concentration increases with increasing n_n, and starting from a certain point the production of Σ^- is energetically more economical than that of one new proton and two new electrons. A similar argument explains why the Ξ^- hyperons appear at lower densities than the Σ^+ hyperons which are lighter than Ξ^-. For $\rho \gtrsim 1.4 \times 10^{17}$ gm/cm^3 the π^- density increases so rapidly with further increase in density that it soon becomes of the order of the densities of the

other members of the mixture.

The general results for the whole region are shown in Figure 2. In order to avoid overcrowding, the hyperons in this graph have been grouped together in a strip. The rise of the densities of these particles is so rapid right after the thresholds have been crossed that the effect of nondegeneracy can safely be neglected. The neutron Fermi energy is about 510 Mev when $n_n \sim 6 \times 10^{38}$ cm^{-3}. All through the region of the hyperon phase the electron number densities are roughly two to three orders of magnitude lower and the μ^- meson number densities are about three to four orders of magnitude lower than the neutron number densities.

Recently, Bahcall and Wolf (1965) raised the question of the presence of pions even near normal nuclear densities ($\sim 4 \times 10^{14}$ gm/cm^3). This is possible only if pions have a sufficiently small effective mass. If protons and neutrons were present with equal abundance, this might be realized. However, both Bahcall and Ruderman, through recent private communications, indicated to one of us (Cameron) their expectations that, under the conditions in which pions may be present in a neutron star (where n_p/n_n is quite small), there will be a predominantly repulsive interaction between the pions and neutrons. This would raise rather than lower the effective mass of the pions, which makes it very

unlikely that pions will be present in neutron stars.

COMPOSITE EQUATION OF STATE

As we go outward from the center of a neutron star, the density decreases from the central value. If the central density is higher than about 10^{15} gm/cm^3, we will have a mixture of hyperons, nucleons, mesons and electrons in the central region, neutron-dominated intermediate layers (with a small admixture of protons and electrons), and outermost layers of electrons and heavy ions. In this section we consider how the pressure depends on density in these complex layers. The equation of state is most conveniently expressed as:

$$P = P_{KE} + P_{PE}; \qquad \epsilon = \epsilon_{KE} + \epsilon_{PE} \qquad (10)$$

where P is the total pressure, ϵ is the total energy density and the subscripts KE and PE stand for the kinetic and potential terms, respectively. The kinetic parts are expressed as

$$\epsilon_{KE} = K_n \sum_k \left(\frac{M_k}{M_n}\right)^4 \frac{a_k}{2} (\sinh t_k - t_k)$$

$$P_{KE} = \frac{K_n}{3} \sum_k \left(\frac{M_k}{M_n}\right)^4 \frac{a_k}{2} (\sinh t_k - 8 \sinh \frac{t_k}{2} + 3t_k)$$

$$(11)$$

where the summation is taken over all particles in (2) which are present, and

$$K_n = M_n^4 c^5 / (32\pi^2 \hbar^3) = 5.117 \times 10^{35} \text{ dynes/cm}^2$$

$$a_k = (2I_k + 1) \quad \text{as given in Equation (5)}$$

$$t_k = 4 \sinh^{-1} \left[\left(\frac{6\pi^2}{a_k} \right)^{1/3} \frac{\hbar}{M_k c} n_k^{1/3} \right] \tag{12}$$

and the remaining notation is that given in the last section.
Each term in Equation (11) corresponds to the partial pressure
or partial energy density (including rest mass energy) of
completely degenerate fermions k of a particular kind, and
applies to both non-relativistic and relativistic particles.

At the present time, the behavior of nuclear forces in
the high energy region is not well known. However, various
models of nuclear potential near the region of nuclear density
have been constructed by different authors (Brueckner and Gammel
1958; Brueckner, Gammel, and Kubis 1960; Sood and Moszkowski
1960; de Swart and Dullemond 1961; Serber 1964; and others). In
this paper, the neutron-neutron potentials as introduced by
Levinger and Simmons (1961) were utilized.

Levinger and Simmons introduced three forms of potential
designated V_α, V_β, and V_γ, but due to the poor fit in our region
of most interest, V_α was not used in this paper. The V_β is a
square well potential with a tail of the Yukawa type, and the
V_γ is a complicated combination of exponentially decreasing

terms which in effect give rise to the same kind of properties

as V_β. Both potentials V_β and V_γ are well behaved, velocity-

dependent, and, with the assumption of charge independence, are

well fitted to the ^1S and ^1D phase shifts from 20 to 340 Mev.

They are utilized in this paper. They consist of static and

velocity-dependent parts of the ordinary and exchange integrals.

The ordinary static term V_o and the ordinary velocity-dependent

term ω_o are given in the analytic forms $-\alpha k_f^3$ and βk_f^5, respec-

tively, where α and β are positive constants (which are

different for V_β and V_γ, and k_f is the Fermi wave number, which

is related to number density by

$$n = k_f^3/(3\pi^2). \qquad \qquad (13)$$

On the other hand, the exchange terms V_e (ordinary) and ω_e

(velocity-dependent) depend on k_f in a complicated way. There-

fore, the potential terms of the equations of state are conveniently

expressed as:

$$\epsilon_{PE} = nV(n) = (-\alpha k_f^3 + \beta k_f^5 + 0.7V_e - 2\omega_e)cn \quad \text{ergs/cm}^3$$

$$P_{PE} = n^2 \frac{\partial V(n)}{\partial n} = \left[\frac{n}{3}\left(-3\alpha k_f^3 + 5\beta k_f^5\right) + n^2\left(0.7\frac{\partial V_e}{\partial n} - 2\frac{\partial \omega_e}{\partial n}\right)\right]c \quad \text{dynes/cm}^2$$

$$(14)$$

where $V(n)$ is the Levinger-Simmons potential energy per particle,

and

$$c = 1.602 \times 10^{-6} \quad \text{ergs/Mev}$$

$$\alpha = 1.3a_1, \quad \beta = 4a_2$$

$$a_1 = 3.02, \quad a_2 = 0.045 \text{ for } V_\beta \quad \text{(Mev)}$$

$$a_1 = 4.02, \quad a_2 = 0.28 \text{ for } V_\gamma \quad \text{(Mev)} \tag{15}$$

The total baryon number density n is

$$n = \sum_b n_b \quad \text{(b denotes all baryons which are present)}. \tag{16}$$

n_b is related to t_b through the last equation in (12). V_e and ω_e were determined numerically in the region $0 \le k_f \le 2$ (Levinger and Simmons 1961). These values were plotted against k_f and the slopes have been used to determine $\dfrac{\partial V_e}{\partial n}$ and $\dfrac{\partial \omega_e}{\partial n}$. For $k_f > 2$, the results were extrapolated. This procedure is justified because V_e and ω_e are negligible for $k_f \gtrsim 3$, as compared with the other terms. (k_f is expressed in f^{-1}, where f is in fermis, 10^{-13} cm.)

The total energy per particle is plotted against density in Figure 3, for the Levinger-Simmons V_β and V_γ potentials, the Skyrme potential and Salpeter's potential. For $10^{13} < \rho < 10^{15}$ gm/cm^3, the potentials are attractive and the total energy is less than the case for the noninteracting particles. For $\rho > 10^{15}$ gm/cm^3, the repulsive terms become dominant. In most of the region of

attractive potential V_γ is somewhat lower than V_β, but the repulsive term of V_γ is much larger than that of the V_β. Nuclear potentials are negligible for $\rho < 10^{13}$ gm/cm^3.

In the above equations, the potential terms were expressed as functions of total baryon number density. This implies that we have applied these potential interactions between baryons without distinction as to the type of baryon. At the present time general baryon interaction potentials are not known properly, so the use of V_β and V_γ in this way corresponds to slowly and rapidly increasing repulsive terms among baryons at high densities.

At densities less than or equal to nuclear density, the character of nuclear forces is reasonably well known and is given to a rough approximation by either of the two potentials adopted here, and the composition of the matter is mostly neutrons, for which the potentials were originally constructed. At much greater than nuclear density many different types of baryons are present, and the rapidity with which nuclear forces turn repulsive is very speculative. Therefore, the two potentials V_β and V_γ tend to span a range of possible behavior of the nuclear forces at high densities and the differences in the neutron star models which result from the adoption of one or the other of these potentials will give an indication of the uncertainty due to lack of knowledge in this field.

In the above equations of state, bosons are not included, because the only bosons considered and listed in (2) are negative pions, which are most unlikely to exist at densities below about 10^{17} gm/cm^3, while the equation of state becomes independent of composition and the above Levinger-Simmons type equations of state cease to be valid long before such high densities are reached. This restriction is imposed due to two reasons. One is that in the case of a perfect fluid there is a relativistic limitation on the pressure that it cannot exceed one-third of the proper energy density (Landau and Lifshitz 1959). The other more general restriction which may apply in a fluid with anisotropic properties is that the pressure cannot exceed the energy density (Zel'dovich 1962). If this were to be violated the speed of sound would exceed the speed of light in the medium. Accordingly, the Levinger-Simmons equations of state were cut off with one of these pressure saturation conditions at the high density limit.

In order to determine the composite equation of state as described above, we must know the equilibrium composition as a function of density. To examine this problem, let us go back to Figure 2. In region (I) the nuclear abundances as calculated in a separate paper (Tsuruta and Cameron 1965) are valid. In the higher density region marked (III) the hyperonic mixture as obtained in the last section applies. Care may have to be taken in dealing

with the intermediate region marked (II). When the density

is about 3×10^{11} gm/cm^3 (the point marked (a) in Figure 2) the

electron Fermi energy is about 23 Mev and nuclei such as ^{120}Sr

will coexist with free neutrons. By the time we arrive at the

border (b), where the density is about 8×10^{13} gm/cm^3, all the

heavy nuclei are expected to have disappeared, leaving neutrons,

protons and electrons in equilibrium. The exact behavior of the

transition in this region is quite complicated, but the same

principles, the conservation of total energy, charge and number

of particles, control the equilibrium in this region. To prevent

a discontinuous change in the ion number densities, it was assumed

that the average charge $\bar{Z}$ changes from 38 to 1 in a smooth way

from point (a) to point (b). Then, the average ionic charge is

expressed as:

$$\bar{Z}(\rho) = 1 + 37 \ \chi(\rho) \tag{17}$$

where

$$\chi(\rho) = \frac{(\rho_2 - \rho)}{(\rho_2 - \rho_1)} \qquad \text{for} \qquad \rho_1 \leq \rho \leq \rho_2 \ .$$

ρ_1 is the density at (a), and ρ_2 is the density at (b).

Strictly speaking electron density increases slightly as we

go from (a) to (b) with an increase of neutron density, but this

rise is negligible and not appreciable in Figure 2. This is

because the major part of the extra energy density as we go from (a) to

(b) goes to neutron density. Figure 2 also indicates that there is a rise in the total ion number density as the average ionic charge changes from 38 to 1.

In the lower density region $\rho \leq 8 \times 10^{13}$ gm/cm^3 it is more convenient if the matter density ρ, as defined below, is used as a free parameter.

$$\rho = \sum_k \left\{ \left[n_n + (A-Z) n_k(A,Z) \right] m_n + \left[n_p + Z n_k(A,Z) \right] m_p \right\} + n_e m_e \qquad (18)$$

k represents all nuclei of appreciable abundance. Then the energy density is expressed as

$$\epsilon = \epsilon_{KE} + \epsilon_{PE} + \rho - n_n m_n - n_p m_p - n_e m_e$$

The rest mass density of p,e,n must be subtracted because both ϵ_{KE} and ρ include them. ϵ_{KE} is given by (11) with k = n,p,e; ϵ_{PE} is given by (14) with n = $n_n + n_p$. The abundances of different particles as a function of density were taken from Tsuruta and Cameron (1965). The expressions for pressure in Equations (10) - (16) are valid in this region with k = n,p,e and n = $n_n + n_p$. The contribution of interactions between electrons is always negligible in the problem of neutron stars (Salpeter 1961) and hence such terms are not included in the above equations. In this low density region the main contributor to pressure is electrons or neutrons. The effect of the presence of heavy nuclei appears in

the density but not in the pressure.

For the region $\rho > 8 \times 10^{13}$ gm/cm^3 the composite equations

of state as described above are most easily solved by choosing t_n,

the relativistic parameter for neutrons as defined in Equation (12),

as our free parameter.

The solid curves in Figure 4 represent the final composite

equations of state of type V_β and V_γ. The nearly straight line

in the lower density region corresponds to the electron-nucleus

configuration. Even though it is not apparent from the graph,

this line is found to be slightly bent downward if we examine it

more carefully, which is due to the decrease of Z/A with the increase

in density in this region. In high density regions ($\rho > 10^{16}$ gm/cm^3)

the asymptotic equation $P = \epsilon$ is seen to be approached. The difference

between the two potentials V_β and V_γ is apparent in the most

interesting region of $10^{13} \leqslant \rho \leqslant 10^{16}$ gm/cm^3.

GENERAL RELATIVISTIC EQUATIONS OF HYDROSTATIC EQUILIBRIUM

The most general static line element exhibiting spherical

symmetry may be expressed in the following form (Tolman 1934):

$$ds^2 = -e^{\lambda(r)} dr^2 - r^2 d\theta^2 - r^2\sin^2\theta \, d\varphi^2 + e^{\nu(r)} dt^2$$

$$(19)$$

For this line element and with the assumption that the matter

supports no transverse stresses and has no mass motion, the general

relativistic equations of hydrostatic equilibrium are expressed

as (Oppenheimer and Volkoff 1939):

$$\frac{dU(r)}{dr} = 4\pi\epsilon r^2 \tag{20}$$

$$\frac{dP}{dr} = -\frac{(P+\epsilon)}{r(r-2U(r))}(4\pi r^3 P+U(r)) \tag{21}$$

where P is the pressure and ϵ is the macroscopic energy density

both measured in proper coordinates, and U(r) is the gravitational

mass contained within a sphere of radius r. The gravitational

mass of the star, M, is obtained by integrating (20) from the

center to R, the radius of the star, where P = 0.

In this section, we use the following system of units unless

otherwise stated: the units for which

$$c = G = 1$$

(c is the velocity of light and G is the gravitational constant),

and

$$\left(\frac{M_n^4 c^5}{32\pi^2 \hbar^3}\right) = K_n = 1/4\pi$$

The quantities in this system of units are converted to those in

cgs units by multiplying them by the following conversion factors:

length: $\qquad r_o = 2\sqrt{2\pi} \left(\dfrac{\hbar}{M_n c}\right)^{3/2} \dfrac{c}{\sqrt{GM_n}} = 1.37 \times 10^6 \text{ cm} = 13.7 \text{ km} \sim 10^{-5} R_\odot$

mass: $\qquad m_o = r_o c^2/G = 1.85 \times 10^{34} \text{ gm} = 9.29 M_\odot$

pressure: $\qquad P_o = (M_n^4 c^5/32\pi^2 \hbar^3) 4\pi = 6.46 \times 10^{36} \text{ dynes/cm}^2$

density: $\qquad \rho_o = P_o/c^2 = 7.15 \times 10^{15} \text{ gm/cm}^3$

The gravitational mass M as defined earlier is the mass of the star as perceived by a distant observer. This differs from the proper mass, which is the mass the star would have if its particles were dispersed to infinity. The proper distance and proper time intervals in a gravitational field are determined from:

$$dr_p = \sqrt{-g_{rr}} \ dr \qquad (22)$$

where

$$- g_{rr}(r) = e^{\lambda(r)} = \left(1 - \frac{2M}{r}\right)^{-1}$$

$$\text{if } r \geq R$$

$$g_{44}(r) = e^{\nu(r)} = \left(1 - \frac{2M}{r}\right)$$

$$- g_{rr}(r) = \left(1 - \frac{2U(r)}{r}\right)^{-1}$$

$$\text{if } r < R$$

$$g_{44}(r) = \left(1 - \frac{2M}{R}\right) \left(\frac{\mu_s}{\mu(r)}\right)^2$$

$$(23)$$

where μ_s is the chemical potential at the surface and $\mu(r)$ is the chemical potential at distance r, which can be expressed as:

$$\mu_s = M(56,26)/56$$

$$\mu(r) = (P + \epsilon)/n \tag{24}$$

$M(56,26)$ is the mass of a free atom of ^{56}Fe, and n is the total baryon number density. The proper mass M_p is obtained by integrating the following differential equation:

$$\frac{dM_p}{dr} = 4\pi\rho r^2 \left(\frac{r}{r-2U(r)}\right)^{1/2} \tag{25}$$

ρ is the matter density as defined by Equation (7) or (18). The total binding energy in mass units M_B is obtained by integrating the following:

$$\frac{dM_B}{dr} = 4\pi r^2 \left[\rho\left(\frac{r}{r-2U(r)}\right)^{1/2} - \epsilon\right] \tag{26}$$

It is evident that the solution of the differential equations (20), (21), (25), and (26) depends only on the equation of state and on the boundary conditions at the center.

Examining the expression of the line element in Equations (19) and (23) we note that the following inequality must be fulfilled for any real solutions:

$$R > R_G = 2GM/c^2 = 2.94 \ (M/M_\odot) \text{ in units of km.}$$

(27)

The limiting radius R_G is called the "gravitational radius".

When $R = R_G$, a singularity occurs. This singularity is called

the Schwarzschild singularity. On this surface, the time metric

vanishes, the curvature of space becomes infinite and no light

emitted from this surface will reach us. Hence, we will face a

serious problem if the solution of the above equilibrium equations

gives rise to a radius less than or equal to the gravitational

radius.

In the problem of neutron stars, another interesting quantity

is the gravitational red shift which is obtained from:

$$\varphi = \frac{\Delta\lambda}{\lambda} = \frac{GM}{Rc^2} = \frac{1.47 \ (M/M_\odot)}{R(km)} = \frac{R_G}{2R}$$

(28)

RESULTS

The equilibrium equations (20), (21), (25), and (26) have

been integrated numerically with the aid of the 7094 computer,

for each of about 120 initial values of central density in the

range $10^6 \leqslant \epsilon^c \leqslant 10^{26}$ gm/cm^3, for each of the composite equations

of state of type V_β and V_γ with the pressure saturation condition

$P \leq \epsilon$. Additional integrations were carried out for the same

composite equations of state but with a different pressure satura-
tion condition, $P \leq \epsilon/3$. The integrations were terminated at
the point where $\log \epsilon = 0$. (ϵ^c is the central energy density.)

The characteristic features of the resulting models of the
type V_β and V_γ with the asymptotic equation of state $P = \epsilon$ are
given in Tables 1 and 2. Similar results were obtained for these
models with the restriction $P \leq \epsilon/3$. The gravitational and
proper masses of these models (both with $P \leq \epsilon$ and $P \leq \epsilon/3$) are
plotted as functions of the central matter density ρ^c in Figure 5.
The points where the respective form of the asymptotic equations
of state start to become applicable are marked by crosses. It is
clear that the individuality of the constituent particles becomes
indistinguishable for $\rho^c \gtrsim 10^{16}$ gm/cm^3. The models lying along
the lower branch of the principal mass peak are stable, while the
models beyond this point are unstable (Tsuruta 1965, Harrison,
Thorne, Wakano and Wheeler 1965). Hence, the effect of the pressure
saturation condition $P \leq \epsilon$ or $P \leq \epsilon/3$ is negligible for most of
the stable neutron stars. However, different assumptions of the
pressure saturation condition give rise to a small shift in the
values of mass, radius, etc., for models near and above the
principal mass peak. A small local mass peak is observed in the
intermediate region between the regions of white dwarfs and neutron
stars. This is the region where we assumed a smooth but crude

dissolution of ions into nucleons. The reality of this small peak is questionable and requires further investigation. We conveniently use the expression "pressure saturation condition" to refer to the phenomenon that the pressure is not allowed to go beyond certain limits which are functions of energy density. "Ideal" gas models refer to models consisting of non-interacting particles, and "real" gas models refer to the models for which some interaction potential between baryons is assumed.

The mass-radius relation for the entire range of central density is shown in Figure 6. The portion marked (I) belongs to the white dwarf region. Around the region marked (II) lie a series of models in the intermediate region where inverse beta processes change the equilibrium composition rapidly with change of density. Around the region marked (III) lie neutron and hyperon stars. The solid curves represent our "real" gas models of V_β and V_γ type, and the dashed curve marked (a) and that marked (b) represent the "ideal" gas and "real" gas models constructed by Ambartsumyan and Saakyan (1962a), respectively. The masses are significantly increased when the nuclear forces are taken into account. In the absence of nuclear forces, the maximum mass of neutron stars is only about 0.67 of the mass of the sun, while it can be as large as twice the solar mass in the presence of nuclear forces.

The radius of the models of type V_β and V_γ is plotted as a function of central energy density in Figure 7. At the points

marked D, the models are as large as some of white dwarfs. The density at the center of these models is about $4 \sim 7 \times 10^{13}$ gm/cm^3. These models have the interesting configuration of a small central core of neutrons (with small concentration of electrons and protons) surrounded by huge envelopes consisting of electrons and heavy nuclei, whose exact composition changes from layer to layer as we approach the surface. We shall call these envelopes "electron-nucleus" envelopes. The possible existence of these extended envelopes of electrons and heavy ions was first suggested by Hamada and Salpeter (1961) and is confirmed in this paper. Other points marked by crosses and letter symbols are some of the critical points as defined in Table 3. The radius-central density relation in the region of neutron and hyperon stars is shown in an enlarged scale in Figure 8. The "ideal" gas models are also shown for comparison. We note that the effect of the presence of nuclear forces on stellar radius is not so significant as that on mass.

We have observed in earlier figures various critical points where major and minor maxima and minima in masses and radius occurred. These points are marked by letter symbols A,B C, etc., in the order of increasing density, in Figure 9. The nature and characteristic features of each critical point are summarized in Table 3. One of the most interesting properties of cold dense stars is that the stellar parameters such as mass, total baryon number, radius,

binding energy, components of metric tensor, etc., exhibit damped

oscillations as functions of central density of the star. To

examine the behavior of these oscillations more closely, the

amplitude fall-off factor and the peak-to-trough separations for

each critical point of the oscillation of mass at sufficiently

high densities were calculated for our models of the V_β and V_γ

type with the asymptotic equation of state $P = \epsilon$. These values are

listed in the last two columns of Table 3. Theoretical values

of these quantities were predicted by Harrison, Thorne, Wakano

and Wheeler (1965) to be

$$\text{Amplitude fall-off factor} = \exp(\pi\alpha/\beta) = 3.95 \text{ for } \gamma = 4/3 (P = \epsilon/3)$$

$$\text{and} = 6.147 \text{ for } \gamma = 2 (P = \epsilon)$$

$$(29)$$

and

$$\Delta \log_{10} \epsilon^c = 2 \times 0.4343 \, \pi/\beta = 1.59 \text{ for } \gamma = 4/3 (P = \epsilon/3)$$

$$\text{and} = 1.578 \text{ for } \gamma = 2 (P = \epsilon),$$

$$(30)$$

where

$$\alpha = \frac{3}{2} - \left(\frac{1}{\gamma}\right)$$

$$\beta = \left[-\left(\frac{9}{\gamma^2}\right) + \left(\frac{11}{\gamma}\right) - \frac{1}{4} \right]^{1/2}, \quad \gamma = \text{the adiabatic exponent}$$

$$(31)$$

At sufficiently high densities the approximation $P = \epsilon$ should be valid for our real gas models of V_β and V_γ shown in Table 3. The agreement between our results and the theoretical values in Equations (29) and (30) is quite satisfactory within the estimated order of accuracy. Figure 9 shows the damped oscillations of radius and mass for the V_γ models with $P \leq \epsilon$. We see that the oscillation of radius is somewhat out of phase with the oscillation of mass.

To show the effect of having a composite hyperonic mixture, the composite models and models calculated for a pure neutron configuration are drawn together in Figure 10. The presence of other subatomic particles lowers the partial pressure of the neutrons, and, consequently, smaller stellar masses are expected for the resulting composite models than for the pure neutron stars. This effect of composition, however, is seen to be very small as compared with some other effects such as the effect of nuclear forces.

The internal distribution of matter is shown in Figure 11 for six models of interest. Their properties are given in Table 4. The models marked (1) contain about 0.2 solar mass and consist of large but condensed cores of neutrons surrounded by large envelopes of electrons and nuclei. The envelopes are about 1/3 in width of the total stellar radius. However, such envelopes

quickly diminish for slightly denser stars of $\sim 4 \times 10^{14}$ gm/cm^3 and

they are never important for models with higher densities. The

internal distribution of matter for stars denser than this is almost

constant until the density goes beyond $\varepsilon^c \sim 10^{17}$ gm/cm^3. For

higher densities matter starts to accumulate near the center and the

deviation from homogeneity becomes serious. For models with

$\varepsilon^c \gtrsim 10^{18}$ gm/cm^3 the additional density appears only at the center,

leaving the rest of the interior practically intact. For instance,

the model of $\varepsilon^c \sim 10^{19}$ gm/cm^3 and that of $\varepsilon^c \sim 10^{24}$ gm/cm^3 with

the same equation of state have practically the same internal and

external structure, except at the center.

The internal distributions of various stellar parameters are

given in Table 5, for two models of type V_γ, the one lying just

below and the other just above the principle neutron mass peak.

It is interesting to note that the binding energy is negative in

the central core but it becomes positive in the outer layers.

The internal distribution of the radial and time metrics - $g_{rr}(r)$

and $g_{44}(r)$ for "ideal" gas models were studied by Ambartsumyan and

Saakyan (1962b). By comparing their results with our results for

the "real" gas models shown in Tables 1, 2, and 5, it is obvious

that the non-Euclidean nature of space is more strongly pronounced

both in the interior and on the surface when nuclear forces are

taken into account.

When the central density of neutron stars is higher than ordinary nuclear densities but is less than about 10^{15} gm/cm^3, they are generally composed of a condensed neutron-dominant core surrounded by thin or negligible envelopes of electron-nuclear configuration. These stars were called neutron star models in our discussion. The stars of densities higher than this consist of a condensed hyperon-dominant core surrounded by thin neutron dominant outer layers. These are called hyperon stars in this paper. The electron-nuclear envelopes are always negligible for these hyperon stars.

DISCUSSION

It may be noted that some of the characteristics of dense stars depend greatly not only on the presence of nuclear forces but also on the exact form of these forces. For instance, both the radii and masses of the V_γ type models of dense neutron and hyperon stars are about twice as large as the corresponding values of the V_β type models. It is most desirable to further improve the nuclear equation of state in the critical region of $10^{14.5} \leqslant \rho \leqslant 10^{16.5}$ gm/cm^3.

It is gratifying that the effect of the exact composition of the hyperonic mixture is so small. Even if the threshold density of the appearance of some of the mesons and hyperons is shifted to as low as ordinary nuclear density, the resulting change of

composition will not seriously affect the major properties of cold

models of neutron and hyperon stars reported in this paper unless

there is a large accompanying change in the interaction potentials.

There are certain physical variables whose values are greatly

affected by the presence of nuclear forces but are relatively

insensitive to the exact form of the nuclear potential. These are

the variables which depend on the ratio of mass to radius. For

instance, the red shifts of both the V_β and V_γ type models are about

two to three times as large as the corresponding values for the

"ideal" gas models. The maximum red shift and the largest

departure from Euclidean space are noted at a point just above

the principal mass peak of the neutron stars (point F in Figures 6

and 9). At this point, the red shift of both the V_β and V_γ type

model is about 0.32 while that of the "ideal" gas model is only about

0.15. The non-Euclidean nature of space is enhanced by a factor

of 2 when either the V_β or V_γ type nuclear potential is included.

However, the departure from the Euclidean characteristics is not

large enough to produce a Schwarzschild singularity for all the

models constructed in this paper. (See Equation (28) and Tables

1 and 2.)

A complicated effect of nuclear forces appears in the property

of binding energy. When the constituent baryons become relativistic

the binding energy, which is the proper mass minus gravitational

mass, becomes negative if nuclear forces are neglected (Tsuruta 1964, Misner and Zapolsky 1964). The same argument does not necessarily apply when the interaction forces enter. Depending on the different assumptions of the nuclear forces, the negative binding may or may not occur. For instance, the binding energy becomes negative for sufficiently dense models of "real" gases constructed by Ambartsumyan and Saakyan (1962b), but all the other nuclear models we have studied (the Levinger-Simmons V_β and V_γ type, and Skyrme type potentials) fail to give negative binding energies for relativistic baryons.

It is interesting to note, however, that a small negative binding of about 1% of the stellar mass occurs in the lower density regions of $10^{12} \leqslant \epsilon^c < 8 - 9 \times 10^{13}$ gm/cm^3, below the nuclear densities. This is caused by the presence of relativistic electrons. At these densities the concentration of neutrons is not sufficiently large to overcome the effect of relativistic electrons.

Some of the properties of cold degenerate stars seem to be independent of the type of equation of state to be adopted. The gravitational mass, the proper mass (or total baryon number) and the binding energy exhibit damped oscillations in phase with each other as functions of central density. Hence the point of tightest binding is also the point of maximum mass and maximum baryon number. We have seen that the stellar radius also oscillates as a function

of central density but the oscillation is partly out of phase with the oscillations of the masses. Other interesting variables, the components of the metric tensor and the red shift, also show similar damped oscillations as the central density is increased. Their oscillations are in phase with each other but are not in phase with the oscillations of either the radius or the mass. These properties are found to be common to all different types of equation of state studied by us.

It may be noted that in the models of mass less than about $0.2M_{\odot}$, the binding energy is much less than 1% of the total mass (Table 1 and 2). Such models are energetically unstable against transformation into iron white dwarfs (Cameron 1959). We have noted that the models lying above the principal mass peak (point F) are dynamically unstable. Hence the stable neutron stars, if observable, are expected to lie in the small range of density corresponding to the region $0.2M_{\odot} \leqslant M \leqslant 2M_{\odot}$. The binding energy is only about 1% of the total stellar mass for the lightest of the stable neutron stars but at the mass peak it is as large as about 20% of the observable mass.

Another outcome which may well be noted is the possible importance of the "electron-nucleus" envelopes in some of the lightest stable neutron stars. The most extended envelopes were seen to occur in unstable regions, but it was shown that some of the

stable neutron stars could have quite an extended envelope also, almost as large as the neutron core itself. The mass contained in such envelopes is negligible. Therefore, any physical variables which depend on radius can be greatly affected by the presence of these envelopes. Red shift is an important stellar parameter in the problem of observation. By neglecting the envelopes of electrons and heavy nuclei, about 50% error in the value of red shift could occur for some of the lightest stable neutron stars.

References

Ambartsumyan, V.A. and Saakyan, G.S.   1960.   Soviet Astronomy, 4, 187.

_____   1962a.   Soviet Astronomy, 5, 601.

_____   1962b.   Soviet Astronomy, 5, 779.

Bahcall, J.N. and Wolf, R.A.   1965.   Phys. Rev. Lett., 14, 343.

Brueckner, K.A. and Gammel, J.L.   1958.   Phys. Rev., 109, 1023.

Brueckner, K.A., Gammel, J.L., and Kubis, J.T.   1060.   Phys. Rev.,
    118, 1095.

Cameron, A.G.W.   1959.   Astrophys. J. 130, 884.

_____   1965.   Nature, 205, 787.

Chandrasekhar, S.   1935.   Monthly Notices of Roy. Astronom. Soc.,
    95, 207.

_____   1939.   Introduction to the study of stellar structure
    (Univ. of Chicago Press, Chicago).

Chiu, H.Y.   1964.   Annals of Phys., 26, 364.

Chiu, H.Y. and Salpeter, E.E.   1964.   Phys. Rev. Lett., 12, 412.

Hamada, T. and Salpeter, E.E.   1961.   Astrophys. J., 134, 683.

Harrison, B.K., Thorne, K.S., Wakano, M., and Wheeler, J.A.   1965.
    Gravitation theory and gravitational collapse (Univ. of
    Chicago Press, Chicago).

Landau, L.D.   1932.   Physik. Zeits. Sowjetunion, 1, 285.

Landau, L.D. and Lifshitz, E.   1959.   The classical theory of
    fields (Addison-Wesley Pub. Co., Reading, Mass.).

Levinger, J.S. and Simmons, L.M.   1961.   Phys. Rev., 124, 916.

Misner, C.W. and Zapolsky, H.S.   1964.   Phys. Rev. Lett., 12, 635.

Morton, D.C.   1964.   Nature, 201, 1308.

Oppenheimer, J.R. and Serber, R.   1938.   Phys. Rev., 54, 540.

Oppenheimer, J.R. and Volkoff, G.M.   1939.   Phys. Rev., 55, 374.

Sahakian, G.S. and Vartaman, Yu. L.   1963.   Nuovo Cimento, 30, 82.

Salpeter, E.E.   1961.   Astrophys. J., 134, 669.

_____   1963.   Presented at the First Texas Symposium on

Relativistic Astrophysics.   Also see Ch. VI #32 of I. Robinson,

A. Schild, and E.L. Schucking's Quasi-stellar sources and gravi-

tational collapse 1965.   (Univ. of Chicago Press, Chicago).

Serber, R.   1964.   Revs. Modern Phys., 36, 649.

Sood, P.C. and Moszkowski, S.A.   1960.   Nucl. Phys., 21, 582.

de Swart, J. and Dullemond, C.   1961.   Bull. Am. Phys. Soc., 6, 269.

Tolman, R.C.   1934.   Relativity, thermodynamics, and cosmology

(Clarendon Press, Oxford).

Tsuruta, S.   1964.   Thesis, Columbia University.

_____   1965.   Nature, 207, 470.

Tsuruta, S. and Cameron, A.G.W.   1965.   Can. J. Phys., 43, 2056.

Zel'Dovich, Ya. B.   1962.   Soviet Physics JETP, 14, 1143.

Zwicky, F.   1938.   Astrophys. J., 88, 522.

_____   1939.   Phys. Rev. 55, 726.

_____   1958.   Handbuck der Physik, (Springer-Verlag, Berlin)

51, 766.

TABLE CAPTIONS

Table 1: Characterisitics of Composite Models of Degenerate Stars

with the Nuclear Potential V_β and the Asymptotic Equation of

State $P = \epsilon$; P^c is the central pressure in dynes/cm^2,

$P_o = (M_n^4 c^5/32\pi^2 \hbar^3)4\pi = 6.46 \times 10^{36}$ dynes/cm^2, ϵ^c is the total

energy density at the center and ρ^c is the total matter density

at the center in gm/cm^3, R is the coordinate radius of the

star, M, M_p, and M_B are the gravitational and proper mass

and the binding energy in mass units, $M_\odot$ is the mass of the

sun, t_n^c is the relativistic parameter for neutrons at the

center, $g_{44}(R)$ is the time metric and $-g_{rr}(R)$ is the radial

metric at the surface.

Table 2: Characterisitics of Composite Models of Degenerate Stars

with the Nuclear Potential V_γ and the Asymptotic Equation of

State $P = \epsilon$; the notation is that introduced in Table 1.

Table 3: Properties of Critical Points; the letters A, B, C, etc.,

denote the various critical points in order of increasing

central density of the models ; MAX. 1, etc., means the first

maximum point, etc.; MIN. 2, etc., means the second minimum

point, etc.; the capital letters in ( ) stand for the names

of the persons who recognized or identified these points

first (C = Cameron, H = Harrison, L = Landau, M = Misner,

O = Oppenheimer, HS = Hamada and Salpeter, T = Tsuruta,

V = Volkoff, WW = Wakano and Wheeler, and Z = Zapolsky); the

models HTWW are models constructed by Harrison, Thorne, Wakano and Wheeler; IDEAL means the models with no nuclear interactions, $(\Delta M_{n-1}/\Delta M_n)$ stands for the amplitude fall-off factor, and $(\Delta LOG\ \epsilon^c)$ means the peak-to-trough separation in the LOG ϵ^c vs $M/M_\odot$ plane. Remaining notation is that introduced in Table 1. The second and third columns explain the nature of the critical points designated A, B, C, etc., the 4th column explains the type of model for which the calculations in the last 5 columns were made, and the last 5 columns give the characteristic properties at these points.

Table 4: This table gives the properties of the models used in Figure 11. The notation is that introduced in Table 1.

Table 5: Internal Distribution of Various Stellar Parameters for two models of the V_γ type. The model (A) is slightly less dense and the model (B) is slightly denser than the configuration of maximum mass. r is the radial distance from the center, $\epsilon(r)$, $t_n(r)$, $-g_{rr}(r)$, and $g_{44}(r)$ are the energy density, relativistic parameter for neutrons, the radial and time metrics, all at the point r from the center. $U(r)/M_\odot$ and $M_p(r)/M_\odot$ are the gravitational and proper mass of matter in solar mass units contained within the radius r, and

$$M_B(r) = M_p(r)-U(r)$$

TABLE 1

p^c/p_o	LOG ϵ^c (gm/cm³)	LOG ρ^c (gm/cm³)	R(km)	$M/M_\odot$	$M_p/M_\odot$	$M_B/M_\odot$	t_n^c	$g_{44}(R)$	$-g_{rr}(R)$	RED SHIFT
10^{-13}	6.95173	6.95167	6.782×10^3	0.66838	0.67001	0.00163	0	0.9997	1.0003	1.45×10^{-4}
5×10^{-12}	8.16160	8.16135	3.721×10^3	1.03641	1.03827	0.00186	0	0.9992	1.0008	4.09×10^{-4}
10^{-10}	9.15375	9.15318	2.185×10^3	1.13933	1.14079	0.00146	0	0.9985	1.0015	7.66×10^{-4}
2.5×10^{-9}	10.2786	10.2774	1.217×10^3	0.92016	0.92067	0.00051	0	0.9978	1.0022	1.11×10^{-3}
2.5×10^{-8}	11.0854	11.0836	7.627×10^2	0.72631	0.72655	0.00024	0	0.9972	1.0028	1.40×10^{-3}
2.5×10^{-7}	12.3145	12.3109	7.113×10^2	0.62594	0.62544	-0.00050	0.2661	0.9974	1.0026	1.29×10^{-3}
2.5×10^{-6}	12.9881	12.9836	1.256×10^3	0.62290	0.62176	-0.00114	0.4621	0.9985	1.0015	7.29×10^{-4}
10^{-5}	13.3880	13.3824	2.283×10^3	0.67250	0.67145	-0.00104	0.6299	0.9991	1.0009	4.32×10^{-4}
2.2×10^{-5}	13.6147	13.6084	4.193×10^3	0.40163	0.40108	-0.00055	0.7490	0.9997	1.0003	1.41×10^{-4}
10^{-4}	14.0439	14.0360	53.00	0.12848	0.12856	0.00008	1.0358	0.9929	1.0072	0.00356
8×10^{-4}	14.5587	14.5456	17.37	0.20809	0.21000	0.00191	1.510	0.9648	1.0365	0.01762
4×10^{-3}	14.9626	14.9404	11.66	0.33606	0.34380	0.00774	2.003	0.915	1.0929	0.0425
2×10^{-2}	15.3844	15.3607	8.829	0.44673	0.46737	0.02064	2.443	0.8512	1.173	0.0744
7×10^{-2}	15.6042	15.5748	6.977	0.62085	0.68233	0.06148	2.613	0.738	1.354	0.131
2×10^{-1}	15.7810	15.7322	6.022	0.82269	0.96081	0.13812	2.749	0.598	1.6704	0.201
7×10^{-1}	16.0216	15.9174	5.184	0.96627	1.19409	0.22782	2.932	0.452	2.211	0.274
2×10^{0}	16.4631	16.1847	4.261	0.91218	1.10643	0.18715	3.1983	0.372	2.688	0.314
7×10^{0}	17.1556	16.5014	3.898	0.78682	0.89163	0.10481	3.5547	0.406	2.459	0.297
4×10^{1}	18.1556	16.8936	4.046	0.75035	0.82474	0.07439	4.089	0.4548	2.201	0.2726
2×10^{2}	19.1556	17.2676	4.086	0.77491	0.86534	0.09043	4.742	0.4424	2.260	0.2788
2×10^{3}	20.1556	17.6391	4.059	0.77210	0.86071	0.08861	5.527	0.4408	2.269	0.2796
2×10^{4}	21.1556	18.0115	4.051	0.77040	0.85806	0.08766	6.4317	0.4408	2.269	0.2796
2×10^{5}	22.1556	18.3847	4.0533	0.77107	0.85938	0.08831	7.4257	0.4408	2.269	0.2796
2×10^{6}	23.1556	18.7586	4.05253	0.771024	0.858841	0.087817	8.4805	0.4406	2.270	0.2797
2×10^{7}	24.1556	19.1329	4.05255	0.770956	0.858720	0.087764	9.5737	0.4406	2.270	0.2797
2×10^{8}	25.1556	19.5074	4.05265	0.771029	0.858255	0.087226	10.6905	0.4406	2.270	0.2797
4×10^{9}	25.4566	19.6202	4.05265	0.771031	0.858259	0.087228	11.030	0.4406	2.270	0.2797

TABLE 2

Note: the two lowest-pressure labels printed at the top of the p^c/p_0 column (1×10^{-14}, 1×10^{-12}) could not be matched to data rows; the 27 data rows below are read across each column.

p^c/p_0	$\log \epsilon^c$ (gm/cm³)	$\log \rho^c$ (gm/cm³)	R (km)	$M/M_\odot$	$M_p/M_\odot$	$M_B/M_\odot$	M_B/M (%)	t_n^c	$g_{44}(R)$	$-g_{rr}(R)$	RED SHIFT
1×10^{-11}	6.28406	6.28403	9.101×10^{3}	0.42483	0.42599	0.00116	0.2738	0	0.9999	1.0001	6.85×10^{-5}
6×10^{-11}	7.65431	7.65416	4.842×10^{3}	0.90802	0.90988	0.00186	0.2048	0	0.9994	1.0006	2.76×10^{-4}
6×10^{-10}	8.97596	8.97546	2.387×10^{3}	1.14596	1.14761	0.00165	0.144	0	0.9986	1.0014	7.06×10^{-4}
6×10^{-9}	9.77921	9.77836	1.591×10^{3}	1.03860	1.03942	0.00082	0.078	0	0.9981	1.0019	9.59×10^{-4}
6×10^{-8}	10.5852	10.5839	1.024×10^{3}	0.84461	0.84499	0.00038	0.045	0	0.9976	1.0024	1.21×10^{-3}
6×10^{-7}	11.3924	11.3902	6.314×10^{2}	0.65904	0.65923	0.00019	0.0288	0	0.9969	1.0031	1.51×10^{-3}
2×10^{-7}	12.2363	12.2328	6.857×10^{2}	0.63057	0.63022	-0.00035	-0.0555		0.9973	1.0027	1.35×10^{-3}
2×10^{-6}	12.9685	12.9641	1.076×10^{3}	0.63119	0.63013	-0.00106	-0.168	0.2482	0.9982	1.0018	8.64×10^{-4}
10^{-5}	13.4482	13.4428	1.776×10^{3}	0.71074	0.70960	-0.00114	-0.1605	0.4550	0.9988	1.0012	5.88×10^{-4}
3.7×10^{-5}	13.8117	13.8052	4.246×10^{3}	0.54908	0.54858	-0.00050	-0.0911	0.6598	0.9997	1.0003	1.29×10^{-3}
10^{-4}	14.0566	14.0495	62.28	0.10583	0.10595	0.00012	0.1135	0.8702	0.995	1.0050	2.50×10^{-3}
5×10^{-4}	14.3779	14.3678	17.78	0.20033	0.20234	0.00201	1.001	1.046	0.967	1.034	0.0166
5×10^{-3}	14.7461	14.7251	12.55	0.76612	0.80792	0.04180	5.46	1.326	0.802	1.247	0.0989
2.5×10^{-2}	15.0358	14.9867	11.90	1.49104	1.66813	0.17709	11.88	1.720	0.631	1.581	0.1844
2×10^{-1}	15.4728	15.3369	9.940	1.95294	2.31678	0.36384	18.60	2.069	0.421	2.374	0.2896
5×10^{-1}	15.7040	15.4906	8.942	1.88475	2.22228	0.33753	17.91	2.546	0.380	2.628	0.3101
10^{0}	15.9015	15.6061	8.273	1.77553	2.05128	0.27575	15.49	2.639	0.368	2.719	0.3158
5×10^{0}	16.5535	15.9218	7.488	1.51917	1.62528	0.10611	7.00	2.936	0.404	2.476	0.2981
5×10^{1}	17.5535	16.3348	7.769	1.44985	1.50706	0.05721	3.94	3.360	0.4512	2.215	0.2744
5×10^{2}	18.5535	16.7237	7.875	1.49956	1.58278	0.08322	5.55	3.840	0.440	2.271	0.280
5×10^{3}	19.5535	17.1055	7.812	1.49311	1.57391	0.08080	5.401	4.442	0.438	2.283	0.2810
5×10^{4}	20.5535	17.4825	7.817	1.48981	1.56864	0.07883	5.247	5.180	0.4396	2.275	0.2802
5×10^{5}	21.5535	17.8583	7.803	1.49134	1.57083	0.07949	5.2322	6.047	0.438	2.283	0.2810
5×10^{6}	22.5535	18.2336	7.801	1.49129	1.57076	0.07947	5.2310	7.015	0.438	2.283	0.2810
5×10^{7}	23.5535	18.6087	7.80088	1.49116	1.57054	0.07938	5.2314	8.052	0.438	2.283	0.2810
5×10^{8}	24.5535	18.9836	7.80105	1.49120	1.57060	0.07940	5.2325	9.134	0.438	2.283	0.2810
5×10^{9}	25.5535	19.3585	7.80100	1.49120	1.57060	0.07940	5.2325	10.244	0.438	2.283	0.2810

TABLE 3

PROPERTIES OF CRITICAL POINTS

POINT	EXPLANATION MASS	COMMENT (NOTATION)	MODEL	$\text{LOG } \epsilon^c$ (gm/cm³)	R (km)	$M/M_\odot$	$\dfrac{\Delta M_{n-1}}{\Delta M_n}$	$\Delta \text{ LOG } \epsilon^c$ (gm/cm³)
A	MAX. 1	WHITE DWARF MASS PEAK (L-HWW)	V_γ	8.95	2.34×10^3	1.15		
			V_β	8.95	2.34×10^3	1.15		
			HTWW	8.4	3.5×10^3	1.2		
B	MIN. 1	LOCAL (TC1)	V_γ	12.675	8.3×10^2	0.622		
			V_β	12.76	9.6×10^2	0.612		
C	MAX. 2	LOCAL (TC2)	V_γ	13.65	2.45×10^3	0.754		
			V_β	13.38	2.25×10^3	0.673		
D		LARGEST ENVELOPE (HS-TC)	V_γ	13.856	5.2×10^3	0.3		
			V_β	13.64	4.55×10^3	0.272		
			HTWW	13.17	3×10^3	0.38		
E	MIN. 2	NEUTRON STAR MAIN TROUGH (HWW)	V_γ	13.925	280	0.095		
			V_β	13.75	260	0.113		
			HTWW	13.3	225	0.18		
F	MAX. 3	NEUTRON STAR PRINCIPAL PEAK (LOV)	V_γ	15.48	9.88	1.953		
			V_β	16.05	5.103	0.973		
			IDEAL	15.59	9.25	0.712		
G	MIN. 3	NEUTRON STAR SECOND TROUGH (MZ-TC1)	V_γ	17.253	7.638	1.43582	8	1.601
			V_β	17.854	3.973	0.738	6.12	1.80
H	MAX. 4	NEUTRON STAR SECOND PEAK (MZ-TC2)	V_γ	18.854	7.828	1.50017	6.16	1.552
			V_β	19.456	4.065	0.7765	6.07	1.602

TABLE 3 (continued)

PROPERTIES OF CRITICAL POINTS

POINT	EXPLANATION MASS	COMMENT (NOTATION)	MODEL	$\text{LOG } \epsilon^c$ (gm/cm³)	R (km)	$M/M_\odot$	$\dfrac{\Delta M_{n-1}}{\Delta M_n}$	$\Delta \text{ LOG } \epsilon^c$ (gm/cm³)
I	MIN. 4	NEUTRON STAR THIRD TROUGH (H-TC)	V_γ	20.406	7.807	1.48976	6.2	1.549
			V_β	21.004	4.050	0.77015	6.47	1.548
J	MAX. 5	NEUTRON STAR THIRD PEAK (TC3)	V_γ	21.955	7.8016	1.49144	6	1.599
			V_β	22.554	4.0529	0.77114	6	1.550
K	MIN. 5	NEUTRON STAR 4th TROUGH (TC4)	V_γ	23.554	7.8009	1.49116	7	1.600
			V_β	24.154	4.0525	0.77096		1.600
L	MAX. 6	NEUTRON STAR 4th PEAK (TC5)	V_γ	25.154	7.80103	1.49120		1.6
			V_β	25.734	4.05265	0.77103		1.58

TABLE 4

	$V_\beta(1)$	$V_\beta(2)$	$V_\beta(3)$	$V_\gamma(1)$	$V_\gamma(2)$	$V_\gamma(3)$
$M/M_\odot$	0.1996	0.9663	0.7710	0.2003	1.9529	1.4912
$R(km)$	18.219	5.1842	4.063	17.79	9.940	7.801
LOG ϵ^c	14.5262	16.0216	23.8546	14.3779	15.4728	23.8546
LOG ρ^c	14.5137	15.9174	19.0202	14.3678	15.3369	18.7216
$t_n^{\ c}$	1.476	2.932	9.242	1.326	2.422	8.374
p^c/p_o	7×10^{-4}	0.7	10^8	5×10^{-4}	0.2	10^8

TABLE 5

INTERNAL DISTRIBUTION

	r (km)	LOG $\epsilon(r)$ (gm/cm³)	$U(r)/M_\odot$	$M_p(r)/M_\odot$	$M_B(r)/M_\odot$	$-g_{rr}(r)$	$g_{44}(r)$	$t_n(r)$
MODEL (A) ν_γ	0	15.1683	0	0	0	1.0000	0.2535	2.25
	1.027	15.164	3.3585×10^{-3}	2.6071×10^{-3}	-7.514×10^{-4}	1.0097	0.2557	2.24
	1.986	15.152	2.3889×10^{-2}	1.8894×10^{-2}	-4.995×10^{-3}	1.0368	0.2616	2.23
	2.984	15.132	7.8235×10^{-2}	7.0328×10^{-2}	-7.907×10^{-3}	1.0838	0.2718	2.20
	4.029	15.101	0.18423	0.16646	-0.01777	1.1559	0.2874	2.16
	4.987	15.062	0.33250	0.31203	-0.02047	1.2448	0.3064	2.11
	5.999	15.010	0.54263	0.52955	-0.01308	1.3638	0.3319	2.05
	7.005	14.941	0.79775	0.81098	0.01323	1.5058	0.3632	1.96
	8.007	14.851	1.0809	1.1452	0.0643	1.6615	0.4001	1.85
	9.003	14.727	1.3637	1.5016	0.1379	1.8076	0.4419	1.70
	10.000	14.539	1.6142	1.8347	0.2205	1.9087	0.4855	1.49
	11.000	13.466	1.7537	2.0254	0.2717	1.8876	0.5295	0.67
	11.2	0	1.7552	2.0275	0.2723	1.86	0.538	0
MODEL (B) ν_γ	0	15.7001	0	0	0	1.0000	0.0429	2.88
	1.061	15.682	1.2364×10^{-2}	6.7476×10^{-3}	-5.616×10^{-3}	1.0356	0.0453	2.86
	2.089	15.632	0.08795	0.05195	-0.03600	1.1418	0.0527	2.80
	3.018	15.561	0.23955	0.16876	-0.07079	1.3056	0.0650	2.72
	4.002	15.463	0.48911	0.37571	-0.1134	1.5637	0.0859	2.61
	5.010	15.340	0.81651	0.69958	-0.1169	1.9258	0.1188	2.46
	6.008	15.193	1.1725	1.1232	-0.0493	2.3564	0.1661	2.28
	7.006	15.007	1.5133	1.6020	0.0887	2.7554	0.2293	2.04
	8.002	14.728	1.7850	2.0325	0.2475	2.9235	0.3040	1.70
	8.91	0	1.901	2.226	0.325	2.702	0.371	0

FIGURE CAPTIONS

Figure 1: Number densities in cm^{-3} of various sub-atomic particles as functions of total matter density in gm/cm^3. The symbols n, p, Λ, Σ^-, Σ^o, Σ^+, Ξ^-, Ξ^o, e, μ^-, n* and p* stand for neutrons, protons, hyperons corresponding to their respective symbols, electrons, negative muons, and neutrons and protons in the first excited state.

Figure 2: The composition distribution used in our composite equation of state. The partial number densities of various constituent particles (in units of cm^{-3}) are plotted as functions of total matter density (in gm/cm^3).

Figure 3: Energy in Mev/particle is plotted against density in gm/cm^3, for various nuclear potentials and for non-interacting particles.

Figure 4: Pressure is plotted against energy density for the composite equations of state of type V_β and V_γ, with the asymptotic equation of state $P = \epsilon$.

Figure 5: The gravitational and proper masses of the models of type V_β and V_γ with the asymptotic equation of state of either $P = \epsilon$ or $P = \epsilon/3$. The points at which the composite equations of state switch over to the asymptotic equations of state are shown by crosses.

Figure 6: The mass-radius relation of the composite models of

the type V_β and V_γ with the pressure saturation condition

$P < \varepsilon$ (solid curves). The points A, B, C, etc., are the

critical points as explained in Table 3. The regions (I),

(II), and (III) are the regions of white dwarfs, the inter-

mediate regions, and the regions of neutron and hyperon stars.

The dashed curves are the "ideal" gas models (a) and "real"

gas models (b) constructed by Amburtsumyan and Saakyan (1962a).

Figure 7: The relation between the radius and central energy

density for the composite models of the V_β and V_γ type. Some

of the critical points in low density regions are shown by

crosses and the corresponding letter symbols as introduced

in Table 3.

Figure 8: The relation between the radius and the central energy

density in the region of neutron stars is shown in detail.

For comparison, the models of "ideal" gases are shown as a

dashed curve, together with the "real" gas models of the

V_β and V_γ type (solid curves).

Figure 9: The damped oscillations of the gravitational mass and

radius as functions of central energy density. The regions

(I), (II), and (III) are those defined in Figure 6. The

points A, B, C, etc., stand for the critical points explained

in Table 3. The peaks and troughs of mass and radius are

shown by the respective marks.

Figure 10: The effect of the presence of hyperons. The models

of the V_β and V_γ type are shown both for the configuration

of pure neutrons (dashed curves) and for the baryonic mixtures

(solid curves).

Figure 11: Internal distribution of energy density for 6 models

whose characteristic properties are listed in Table 4. The

solid curves represent the V_γ type models and the dashed

curves represent the V_β type models. These were selected

from (1) the region of the lightest stable neutron stars,

(2) the region near the principal mass peak (point F in

Figure 9), and (3) the region of superdense stars with

$\varepsilon^c \sim 10^{24}$ gm/cm^3.
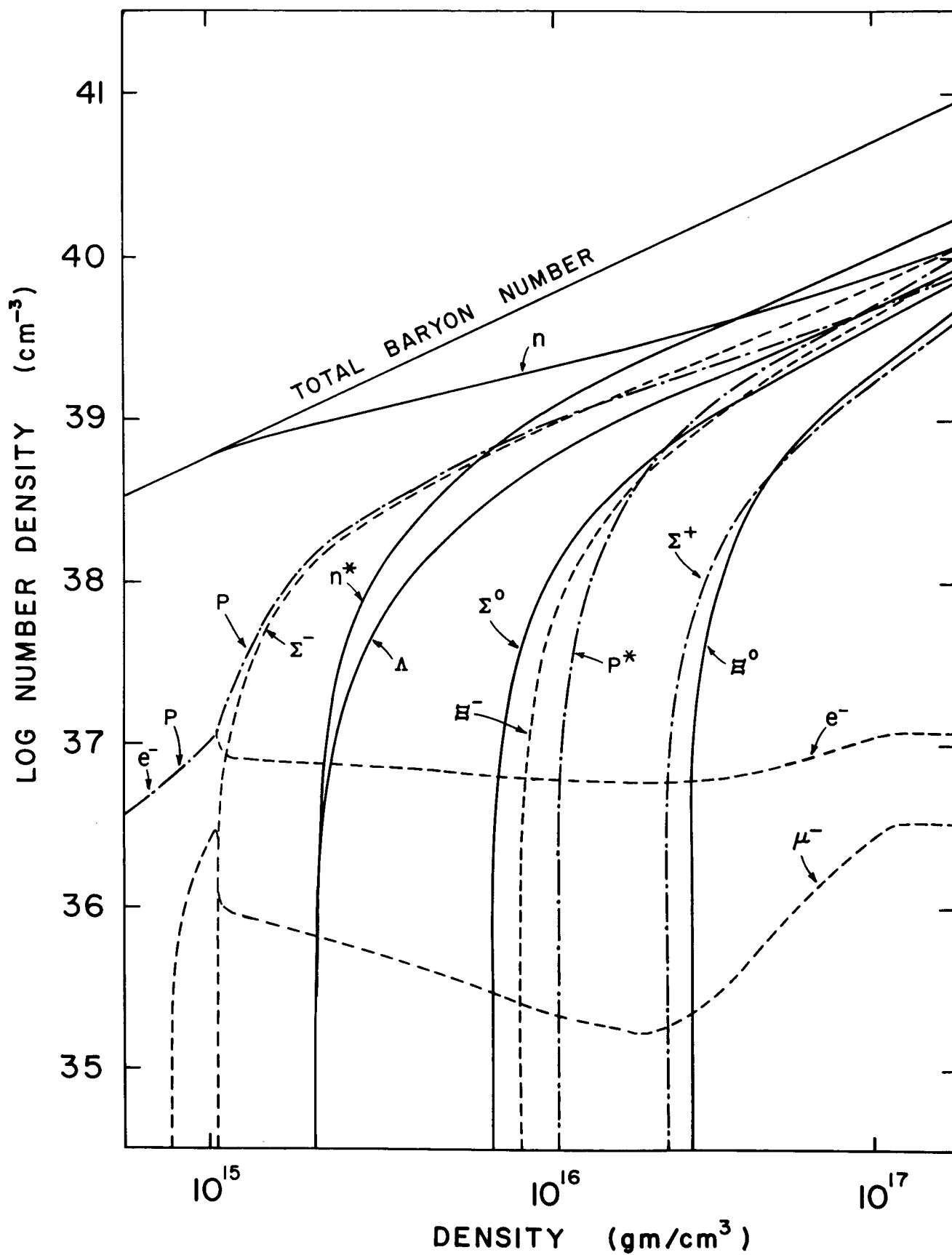
Fig. 1
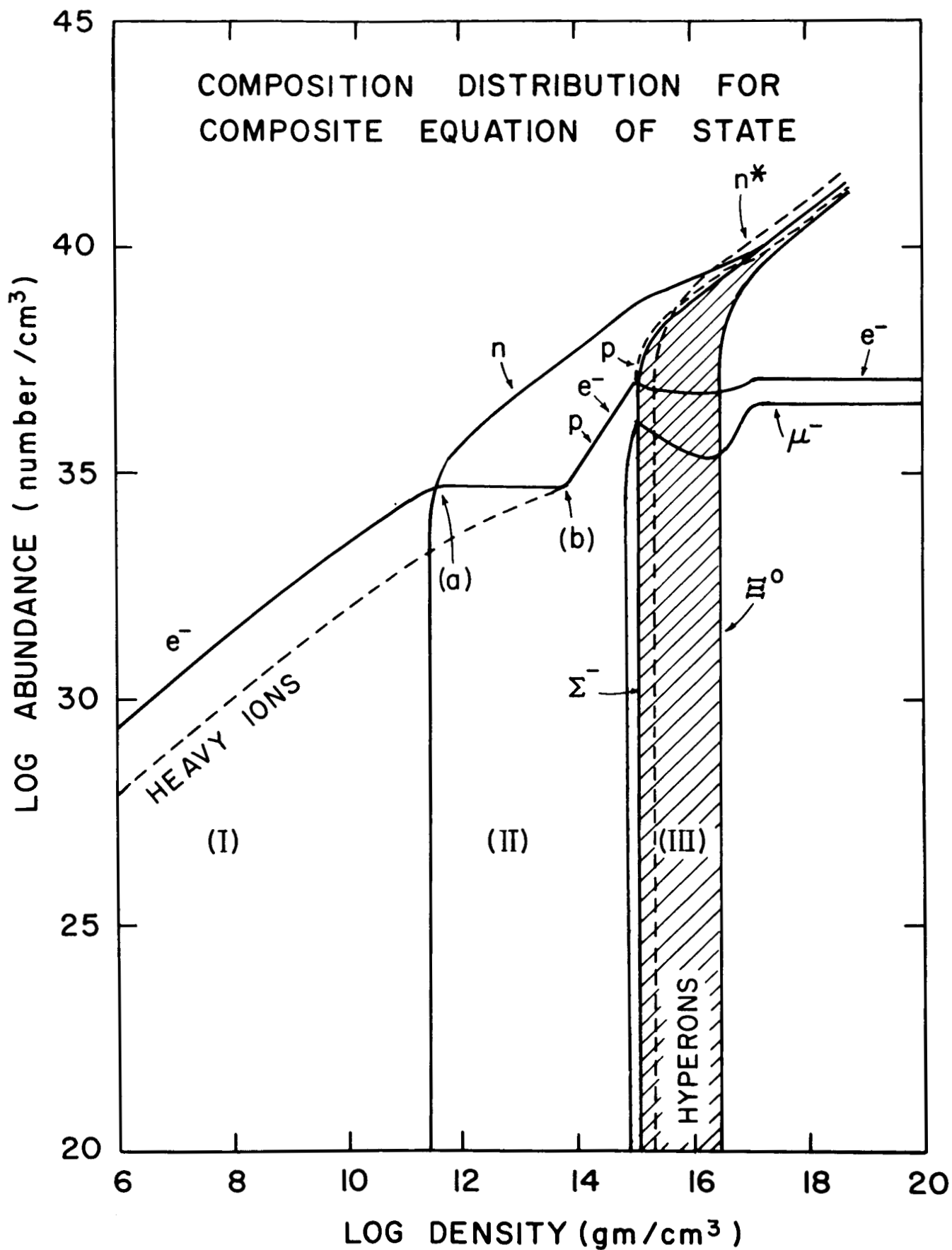
Fig. 2
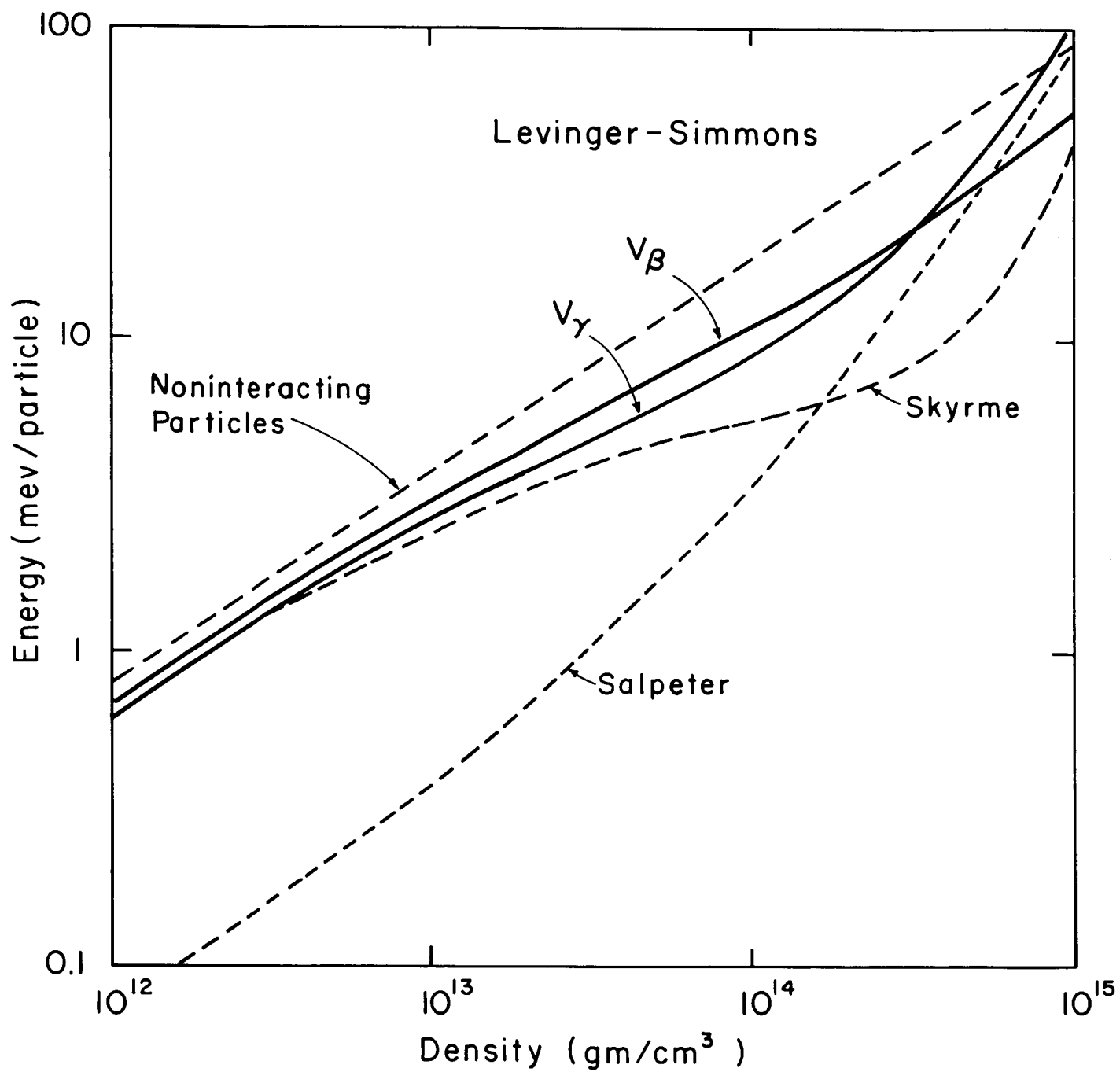
Fig. 3
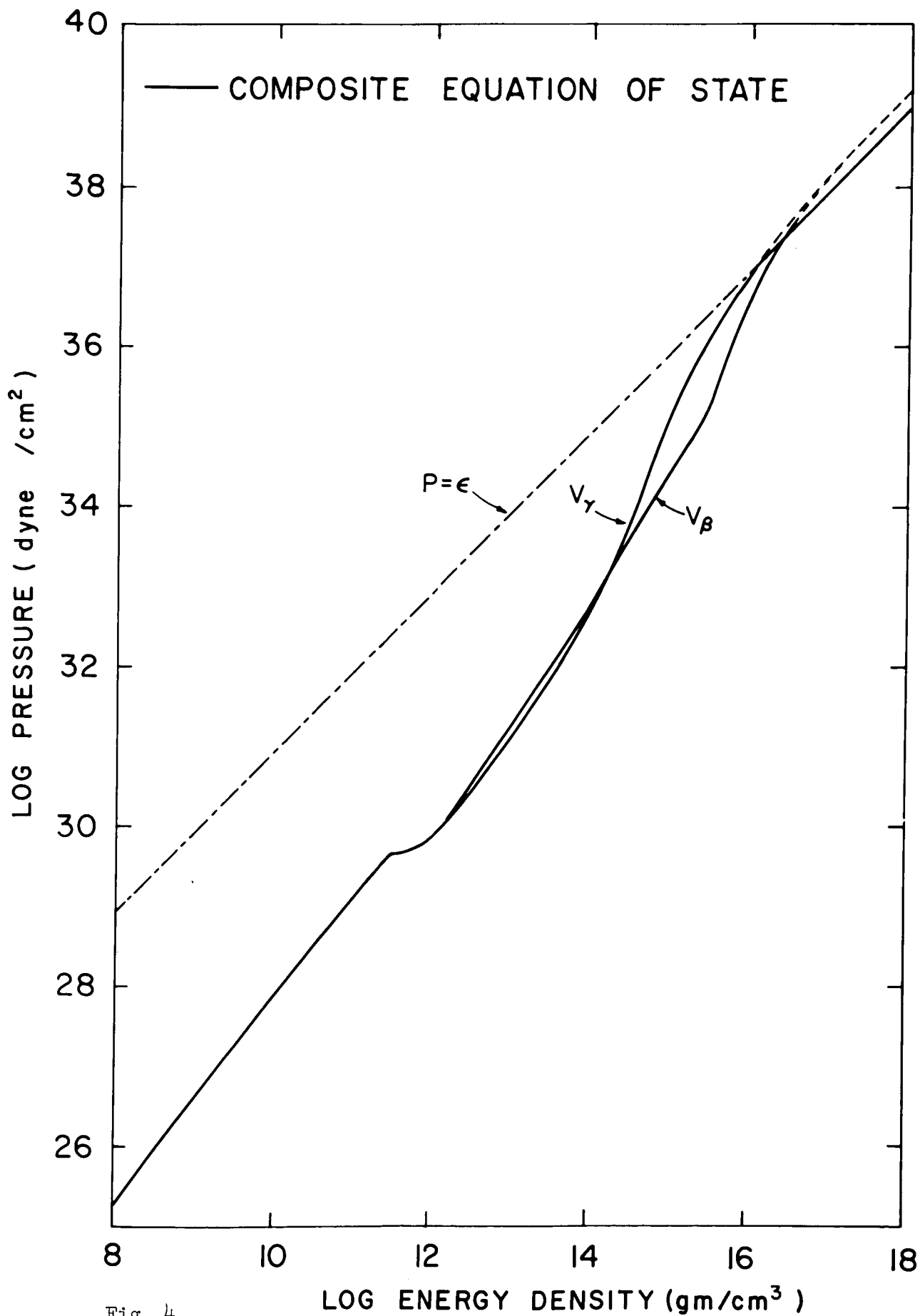
Fig. 4

Fig. 5

Fig. 6

Fig. 7

Fig. 8

Fig. 9

EFFECT OF HYPERONS
—— COMPOSITE
--- PURE NEUTRON

V_β

V_γ

MASS (M/M$_\odot$)

LOG CENTRAL ENERGY DENSITY (gm/cm^3)

Fig. 10

Fig. 11

RADIAL DISTANCE θ (km)

LOG ENERGY DENSITY (gm/cm³)

$V_B(1)$

$V_\gamma(1)$

$V_\gamma(2)$

$V_\gamma(3)$

$V_B(2)$

$V_B(3)$